Green Chemistry

PAPER

View Article Online
View Journal

Open Access Article. Published on 08 December 2025. Downloaded on 1/7/2026 10:12:59 AM.
This article is licensed under a Creative Commons Attribution 3.0 Unported Licence.

Check for updates

Cite this: DOI: 10.1039/d5gc05054e

# $H_2$-driven biocatalytic *O*-demethylation of lignin derived aromatics in a closed-loop flow system powered by water electrolysis

Donato Calabrese,†[a] Guiyeoul Lim,†[a] Parsa Nayyara,[b] Megan E. Wolf,[b] Paul R. F. Cordero,[a] Lindsay D. Eltis*[b] and Lars Lauterbach*[a,b,c]

Received 24th September 2025,
Accepted 1st December 2025

DOI: 10.1039/d5gc05054e

rsc.li/greenchem

Lignin is an abundant and renewable source of aromatic compounds, yet its utilization remains limited due to its recalcitrance and heterogeneity. Recent developments have enabled the catalytic fractionation of lignin into low molecular weight aromatics, which may be transformed into higher-value compounds. Here, we present a scalable biocatalytic platform for the selective *O*-demethylation of lignin-derived aromatic compounds, which integrates an $O_2$-tolerant, $NAD^+$-reducing soluble hydrogenase from *Cupriavidus necator* for cofactor regeneration and NADH-dependent cytochromes P450 and Rieske-type monooxygenases. The process was implemented in a closed-loop flow system featuring dialysis membrane-entrapped multi-enzyme modules. $H_2$ and $O_2$ were precisely supplied *via* gas addition modules powered by water electrolysis. This configuration achieved >99% substrate conversion, high atom efficiency, and effective real-time management of the inhibitory byproduct formaldehyde. The hydrogenase-based cofactor regeneration system exhibits robust tolerance to formaldehyde and is adaptable to a broad range of gas-dependent biocatalytic processes, thereby advancing green, resource-efficient chemical production from renewable biomass.

### Green foundation

1. A sustainable *O*-demethylation system was developed for lignin valorization by leveraging three oxidoreductase systems. By coupling $H_2$-driven cofactor regeneration in a flow setup, this work demonstrates that lignin valorization can be driven by renewable electricity, with minimal waste and high selectivity.
2. The described process utilizes enzymatic catalysis to facilitate the *O*-demethylation of LDACs from renewable lignin biomass under mild reaction conditions. It achieves high product yields (>99% substrate conversion), and incorporates water electrolysis to enable an electro-driven process.
3. Future work could focus on reutilizing formaldehyde (a byproduct), broadening substrate scope, and integrating further gas-dependent oxidoreductases.

## Introduction

Lignin is a highly abundant biopolymer that constitutes up to 40% of lignocellulosic biomass.[1,2] As the demand for sustainable alternatives to fossil fuels grows, the carbon-rich aromatic polymer has been increasingly regarded as a resource for platform chemicals.[1,3–7] Despite its potential, lignin remains largely underutilized in industrial applications due to its structural complexity, heterogeneity, and recalcitrance.[8,9] Given the lack of cost-effective methods to transform lignin into high-value products, the majority is burned for heat and power.[2] The fractionation of lignin biomass yields heterogeneous mixtures of lignin-derived aromatic compounds (LDACs), which are particularly promising substrates for biocatalytic processes.[10] Techniques such as reductive catalytic fractionation (RCF) efficiently break down lignin into LDACs such as alkylguaiacols, *para*-methoxybenzoic acids, and vanillic acid.[11–14] As lignin is highly methoxylated, the majority of LDACs contain at least one methoxy group. LDACs can be transformed into valuable targets by chemical methods including hydrodeoxygenation, oxidative cleavage, and *O*-demethylation.[15,16] However, these methods typically require harsh conditions, often involving high temperatures and pressures and the use of corrosive reagents.[17–22] For example, *O*-demethylation *via*

[a]Institute of Applied Microbiology – iAMB, RWTH Aachen University, Worringer Weg 1, Aachen 52074, Germany. E-mail: lars.lauterbach@iamb.rwth-aachen.de
[b]Department of Microbiology and Immunology, Life Sciences Institute, BioProducts Institute, The University of British Columbia, 2350 Health Sciences Mall, Vancouver, V6T 1Z3, Canada. E-mail: leltis@mail.ubc.ca
[c]Fraunhofer Institute for Molecular Biology and Applied Ecology IME, Forckenbeckstr. 6, 52074 Aachen, Germany
†These authors have contributed equally to this work.

Open Access Article. Published on 08 December 2025. Downloaded on 1/7/2026 10:12:59 AM.
This article is licensed under a Creative Commons Attribution 3.0 Unported Licence.

acid hydrolysis typically requires high temperatures (120–180 °C), pressurized systems, and strongly acidic conditions (pH < 1). This results in substantial energy input and the formation of corrosive acidic waste, complicating downstream neutralization and purification steps.[17] These challenges result in low selectivity, increased operational costs, and limited scalability. An alternative strategy for *O*-demethylation is biocatalysis, whereby enzymes are used under mild conditions to achieve high selectivity (Fig. 1).[23–27] Enzymes that catalyze the *O*-demethylation of LDACs include cytochromes P450 (P450s) and Rieske-type oxygenases (ROs).[25–33] Both classes of oxygenases are widely distributed in bacteria, enabling growth on a variety of LDACs. For example, *Rhodococcus jostii* RHA1 (RHA1) harbours AgcAB and PbdAB, two-component P450 systems that *O*-demethylate alkylguaiacols (**1a**) and *p*-methoxybenzoates (**2a**),[24,27] respectively (Fig. 2A). In these systems, AgcB and PbdB are reductases that contain a [2Fe-2S] ferredoxin and a flavin-binding domain, while AgcA and PbdA are heme-containing monooxygenases. Similarly, RHA1 and *Pseudomonas putida* KT2440 (KT2440) utilize VanAB, a two-component RO that catalyzes the *O*-demethylation of vanillate (**3a**).[34,35] In analogy to the P450 systems, VanA and VanB are oxygenase and reductase components, respectively.

A potential complication of biocatalytic *O*-demethylation is the formaldehyde that is produced. More specifically, *O*-demethylation by P450s and ROs generates one equivalent of formaldehyde (Fig. 2A).[23] Formaldehyde is an electrophilic and protein-reactive molecule that inactivates enzymes through covalent modification of nucleophilic residues such as cysteines, lysines and histidines.[36] The inactivation of the enzymes reduces the efficiency and operational stability of the biocatalytic process. Ultimately, this can hinder conversion efficiency and poses scalability challenges.[37] Enzymatic *O*-demethylation reactions typically rely on electron transfer from reduced cofactors like NAD(P)H.[38] These cofactors are required in stoichiometric amounts to sustain enzymatic activity and can significantly increase operational costs.[38,39] Enzymatic cofactor regeneration systems such as formate dehydrogenase (FDH) and glucose dehydrogenase (GDH) have been utilized to mitigate the high costs of cofactor supply, but recycling requires auxiliary organic substrates and generate byproducts.[40] In contrast, an approach which utilizes "soluble" $NAD^+$-reducing hydrogenase (SH), is atom-efficient and produces no unwanted byproducts.[41–45] This enzyme reduces $NAD^+$ to NADH using molecular hydrogen ($H_2$).[46,47] More specifically, SH oxidizes $H_2$ at the Ni–Fe center and transfers electrons through a series of Fe–S clusters to an FMN-binding domain, where $NAD^+$ is reduced.[48] Unlike most hydrogenases, which are deactivated by trace amounts of molecular oxygen ($O_2$), SH from *Cupriavidus necator* is highly $O_2$-tolerant and has thus been incorporated into many biocatalytic systems for cofactor regeneration.[48,49] Indeed, SH an ideal partner for $O_2$-dependent enzymes such as P450s and ROs (Fig. 1). The integration of SH-mediated cofactor regeneration with the electrochemical production of $H_2$ and $O_2$ further facilitates electro-driven biocatalysis. Thus, water electrolysis generates $H_2$ and $O_2$, which are required for SH-coupled and $O_2$-dependent enzymatic processes, respectively. Although $H_2$ and $O_2$ can be produced *in situ* using a two-electrode system, this method showed low faradaic efficiency, required highly acidic conditions, and exhibited low liquid-to-liquid gas transfer efficiency.[41] *Ex situ* water electrolysis using a proton exchange membrane (PEM) electrolyzer is more energy-efficient, producing $H_2$ and $O_2$ with >60% voltage efficiency and >95% faradaic efficiency. A practical and safe strategy for introducing electrolytically generated gases into biocatalytic flow systems involves the integration of gas-permeable tubing into a closed-loop setup. This configuration enables continuous and controlled delivery of $H_2$ for cofactor regeneration while preventing enzyme deactivation.[42,50] Another strategy for whole-cell catalysis is to use the culture broth directly as catholyte during water splitting, providing $H_2$ to the cells without gas-phase transfer. This has been demonstrated in zero-gap electrolysis systems, for example with *Cupriavidus necator* producing isopropanol from $CO_2$, in hybrid setups coupling a zero-gap cell

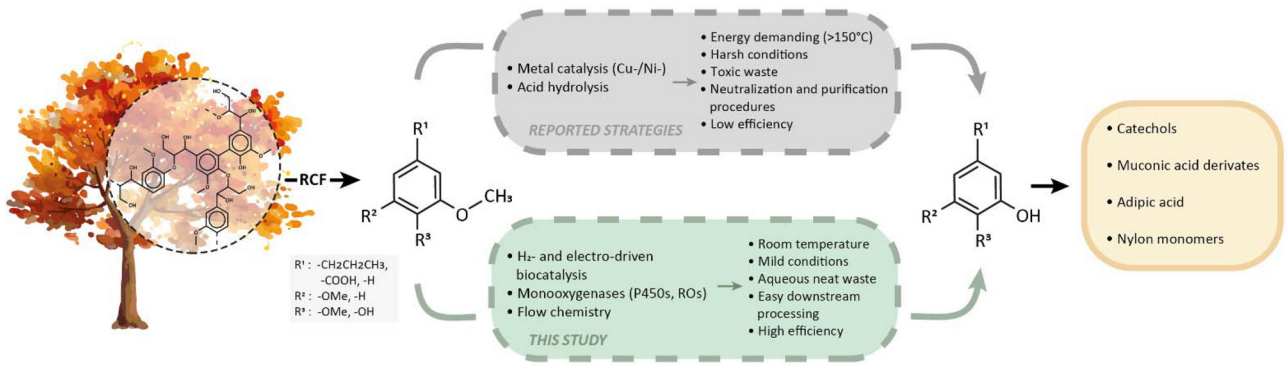


**Fig. 1** Schematic representation of the lignin valorization pathway. In grey, the typical LDACs (lignin-derived aromatic compounds) valorization strategies reported in the literature, based on metal catalysis or acid hydrolysis. In green, our proposed biocatalytic approach for LDACs valorization using $H_2$- and electro-driven systems under mild conditions. $R^1$, $R^2$, and $R^3$ denote typical, yet not exhaustive, substituents found in LDACs. RCF: reductive catalytic fractionation.

Open Access Article. Published on 08 December 2025. Downloaded on 1/7/2026 10:12:59 AM.
This article is licensed under a Creative Commons Attribution 3.0 Unported Licence.

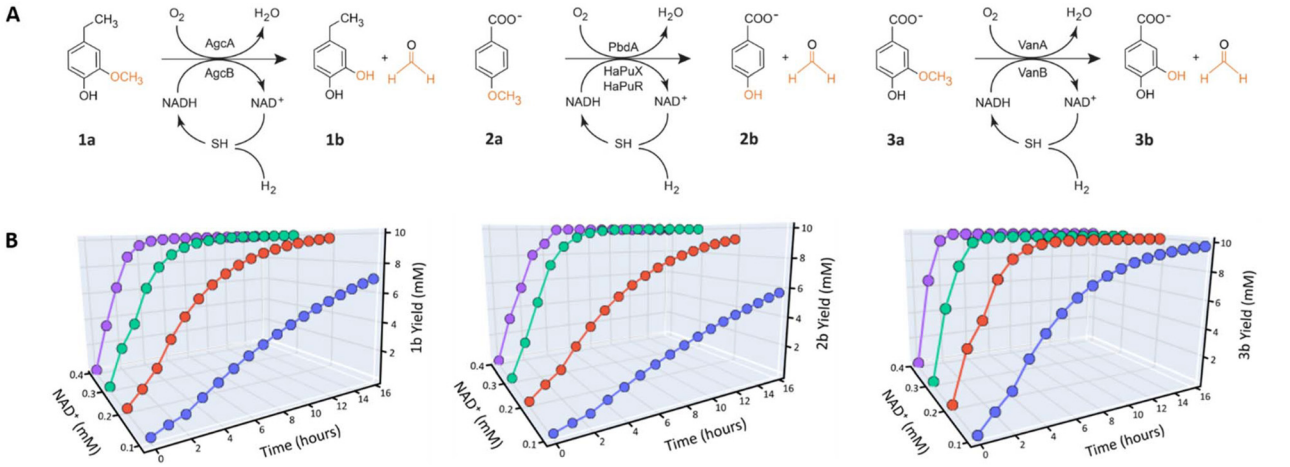


C

| Entry | Enzymes | Product | NAD+ (mM) | $TTN_{Ox}$ | $TTN_{SH}$ | $TTN_{NAD+}$ | Yield (%) |
|---|---|---|---|---|---|---|---|
| 1 | AgcA AgcB | 1b | 0.1 | 1398 | 2796 | 70 | 70 |
| 2 | | | 0.2 | 1946 | 3892 | 49 | 97 |
| 3 | | | 0.3 | 2000 | 4000 | 33 | > 99 |
| 4 | | | 0.4 | 2000 | 4000 | 25 | > 99 |
| 5 | PbdA HaPuX HaPuR | 2b | 0.1 | 568 | 2272 | 57 | 57 |
| 6 | | | 0.2 | 920 | 3680 | 46 | 92 |
| 7 | | | 0.3 | 997 | 3988 | 33 | > 99 |
| 8 | | | 0.4 | 1000 | 4000 | 25 | > 99 |
| 9 | VanA VanB | 3b | 0.1 | 973 | 3892 | 97 | 97 |
| 10 | | | 0.2 | 1000 | 4000 | 50 | > 99 |
| 11 | | | 0.3 | 1000 | 4000 | 33 | > 99 |
| 12 | | | 0.4 | 1000 | 4000 | 25 | > 99 |

**Fig. 2** Comparative analysis of $H_2$-driven *O*-demethylation reactions. (A) Reaction schemes of the three studied monooxygenase systems. Batch reactions were carried out in 8 mL gas-tight vials, each containing 1 mL of reaction mixture prepared in 20 mM phosphate buffer (pH 8.0) with 0.1–0.4 mM $NAD^+$, 10 mM substrate, and enzyme concentrations optimized for each system (5 μM for AgcA and AgcB, 10 μM for VanA and VanB, 10 μM for PbdA, 5 μM for HaPuX, 1 μM for HaPuR, and 2.5 μM for SH). **1a** was used as the substrate for AgcA/AgcB, **2a** for PbdA/HaPuX/HaPuR, and **3a** for VanA/VanB. Gas mixtures: 4% $H_2$, 20% $O_2$, and 76% $N_2$. All reactions were performed using $H_2$ as the sole electron source. (B) Time-course profiles of product formation over 16 hours at different $NAD^+$ concentrations (0.1–0.4 mM). From left to right, the 3D plots represent AgcA/AgcB, PbdA/HaPuX/HaPuR, and VanA/VanB, respectively. (C) Summary table of reaction performance across the tested $NAD^+$ concentrations. The table includes the final product yield (mM), total turnover numbers for the oxygenases ($TTN_{Ox}$: $n_{product}/n_{oxidoreductase}$), soluble hydrogenase ($TTN_{SH}$: $n_{product}/n_{SH}$), and $NAD^+$ ($TTN_{NAD^+}$: $n_{product}/n_{NAD^+}$).

to methanogens using wastewater-derived catholyte, and in water-splitting biosynthetic platforms where electrochemically generated $H_2$ drive $CO_2$ conversion with high efficiency.[51–53]

Here, we report a scalable biocatalytic system for the electro-driven valorization of LDACs by integrating *O*-demethylation with $H_2$-driven NADH regeneration using SH. The valorization potential of three LDAC *O*-demethylase systems, AgcAB, PbdA/HaPuXR, and VanAB, was assessed. To address formaldehyde accumulation and process scalability, the reactions were adapted to a closed-loop flow setup with continuous formaldehyde removal *via in situ* evaporation. The setup incorporates immobilized and entrapped enzymes, enhancing enzyme stability, reusability, simplifying downstream processing, and improving control over formaldehyde production.[53–56] The system was optimized to operate safely and efficiently under non-flammable $H_2$ concentrations.

Open Access Article. Published on 08 December 2025. Downloaded on 1/7/2026 10:12:59 AM.
This article is licensed under a Creative Commons Attribution 3.0 Unported Licence.

Tubing with different gas permeability was integrated into the flow system to precisely regulate the release of $H_2$ and $O_2$ to the reactor. This study showcases the potential for lignin valorization as well as the future broader application of these systems for NAD(P)H- and $FMNH_2$-dependent oxidoreductase reactions,[57] offering a scalable and sustainable pathway for biocatalytic chemical production.

# Experimental section

### Preparation of P450s and ROs

*O*-Demethylase components were produced as His-tagged proteins in *Escherichia coli* BL21 (DE3). AgcA and AgcB from *Rhodococcus rhodochrous* EP4 (EP4) were produced using pET15a.[27] VanA and VanB from KT2400, PbdA from RHA1, and HaPuX and HaPuR from *Rhodopseudomonas palustris* were produced using pET28a.[24,34] Expression was induced in cultures at an $OD_{600}$ of 0.6–0.7 using IPTG. Cell pellets were harvested by centrifugation and stored at −80 °C until use. Proteins were purified using Ni-NTA affinity chromatography (Thermo Scientific), and protein purity was verified by SDS-PAGE. Protein concentrations were determined using BCA Protein Quantification Assay (SERVA). Detailed purification protocols, including buffer compositions and reconstitution procedures, are provided in the SI.

### Preparation of SH

SH from *C. necator* was homologously produced using cells harboring the pGE771 plasmid.[48] Cultures were grown heterotrophically in a mineral salt medium supplemented with fructose, glycerol, trace elements, and metal ions. Cells were harvested by centrifugation and lysed anaerobically using a French press. SH was purified using a Strep-Tactin XT 4Flow column (IBA), and protein purity and concentration were verified by SDS-PAGE and the BCA Protein Quantification Assay (SERVA). Detailed protocols, including media composition, buffer formulations, and purification procedures, are provided in the SI.

### Gas composition reactions setup and analysis

The batch reactions were conducted in 8 mL gas-tight vials, each containing 1 mL of a reaction mixture composed of 20 mM HEPES, pH 8.0, 1 mM $NAD^+$, and 10 mM substrate. Enzyme concentrations were 5 μM AgcA, 5 μM AgcB, 10 μM VanA, 10 μM VanB, 10 μM PbdA, 5 μM HaPuX, 1 μM HaPuR, and 2.5 μM SH. The gas headspace composition was controlled using a gas mixing station (SI section S3.2). The $O_2$ concentration was kept constant at 20%, while $H_2$ concentrations were varied from 2% to 20% in increments of 2%, with nitrogen comprising the remaining balance. The vials were bubbled with the gas mixture before sealing with gas-tight septa. Reactions were initiated by adding enzymes *via* a gas-tight syringe, followed by incubation at 30 °C with shaking at 200 rpm. After overnight incubation, 50 μL samples were quenched 1 : 1 with acetonitrile and analyzed by HPLC. Product formation was quantified using UV absorbance by comparing peak areas to standard compounds. Detailed HPLC protocols, including column specifications, gradient settings, and wavelength monitoring, are provided in the SI.

### Batch reactions setup and analysis

Time-course experiments were performed in 8 mL gas-tight vials containing 20 mM HEPES, pH 8.0, 0.1–0.4 mM $NAD^+$, and 10 mM substrate (ethylguaiacol, **1a**, for AgcAB, vanillate, **2a**, for VanAB, and methoxybenzoate, **3a**, for PbdA/HaPuXR) with a final volume of 1 mL. Enzyme concentrations were 5 μM AgcA, 5 μM AgcB, 10 μM VanA, 10 μM VanB, 10 μM PbdA, 5 μM HaPuX, 1 μM HaPuR, and 2.5 μM SH. The vials were bubbled with a gas mixture containing 4% $H_2$, 20% $O_2$, and 76% $N_2$, sealed with gas-tight septa, and reactions were initiated by adding the enzymes *via* a gas-tight Hamilton syringe. Reactions were incubated at 30 °C with shaking at 200 rpm, and samples were collected hourly for 16 h. Each sample was quenched 1 : 1 with acetonitrile and stored on ice before HPLC analysis as previously described. Formaldehyde formation was monitored over time *via* derivatization with 2,4-dinitrophenylhydrazine (DNPH), followed by GC-FID analysis. Detailed methods are provided in the SI.

### Formaldehyde resistance analysis

The formaldehyde tolerance of the enzyme systems was assessed by conducting $NAD^+$ reduction (for SH) and NADH oxidation (for AgcA/AgcB, PbdA/HaPuX/HaPuR and VanA/VanB) assays in 2 mL quartz cuvettes, using a Cary 60 UV-Vis spectrophotometer. For comparison, a commercially available FDH from *Candida boidinii* (Merck) was used as an alternative $NAD^+$ reducing system. Reactions were maintained at 30 °C, with the following enzyme concentrations: 2.5 μM for SH, 5 μM for AgcA/AgcB, 10 μM for VanA/VanB, 10 μM for PbdA, 5 μM for HaPuX, and 1 μM for HaPuR. Formaldehyde concentrations were varied between 2 and 20 mM, with 0.4 mM $NAD^+$ used in SH reactions and 0.4 mM NADH used in oxidoreductase assays. Reactions were initiated by adding the enzymes directly into the cuvette. Progress was monitored by measuring absorbance at 365 nm, using an extinction coefficient of 3.3 $mM^{-1}$ $cm^{-1}$ for NADH/$NAD^+$ quantification. Reaction slopes were recorded, and enzyme activities were normalized relative to activity in the absence of formaldehyde.

### Electro-driven biotransformation with immobilized enzymes

The reaction was carried out in a closed-loop flow system scaled to 200 mL volume using a peristaltic pump. $H_2$ and $O_2$ were produced using a lab-scale PEM electrolyzer (H-TEC education) operated at 3.9 V and 2.21 A ($H_2$ 33 mL $min^{-1}$, $O_2$ 16 mL $min^{-1}$) for 5 min before addition of aromatic substrate. Approximately 3.8 h (228 min) after substrate addition, the PEM electrolyzer was operated at 3.5 V and 1.03 A ($H_2$ 21 mL $min^{-1}$, $O_2$ 10 mL $min^{-1}$) to ensure full conversion of substrate. $H_2$ and $O_2$ were directly transferred into the flow volume *via* gas addition modules using polyvinylmethyl siloxane (PVMS) and polytetrafluoroethylene (PTFE) tubing, respectively. The

Open Access Article. Published on 08 December 2025. Downloaded on 1/7/2026 10:12:59 AM.
This article is licensed under a Creative Commons Attribution 3.0 Unported Licence.

different permeabilities and lengths of these tubings, described in the SI, enable precise and controlled gas delivery. The reaction medium, containing 50 mM vanillate and 0.3 mM $NAD^+$ in 20 mM Tris-HCl, pH 8.0 at 30 °C, was pumped through the system at 3 mL $min^{-1}$. A flow Clark-type $H_2$ sensor (Unisense) and an optical $O_2$ sensor (PreSens) were added to the flow setup to allow online monitoring of dissolved gases to maintain safe $H_2/O_2$ concentrations. SH and catalase (TCI chemicals) were immobilized on Amberlite FPA54 resin through non-covalent adsorption, at 1 mg SH and 5000 U catalase per gram of resin. This resin was packed into a C10/10 column (Cytiva) as a cofactor regeneration unit with a bed volume of 4 mL. VanAB were contained in a semi-permeable 5 kDa dialysis membrane (Carl Roth) and immersed in a 250 mL Schott bottle with magnet inside for increased diffusion as a biotransformation unit. The temperature of the biotransformation unit was maintained at 30 °C with a hot plate. The cap of the biotransformation unit was opened during the first 2 hours of the reaction for evaporation of formaldehyde. Thin-layer chromatography (TLC) and high-performance liquid chromatography (HPLC) were used to monitor reaction progress, and formaldehyde levels were determined by gas chromatography. At the end of the reaction, the product was extracted with ethyl ether, dried, and crystallized for further analysis by NMR. Details are provided in the SI.

## Results and discussion

### Benchmarking safe and efficient $H_2$-driven *O*-demethylation

The enzymatic transformation of LDACs offers a promising strategy for converting renewable biomass into value-added chemicals. We selected three representative *O*-demethylases to further explore the biocatalytic potential of these enzymes: AgcAB from EP4, VanAB from KT2440, and PbdA from RHA1 paired with HaPuX and HaPuR from *R. palustris*. HaPuX and HaPuR, the ferredoxin and ferredoxin reductase, respectively, from a homologous P450 system, were used instead of PbdB due the $O_2$-lability of the cognate reductase (SI Table S3).[24] Similarly, AgcAB from EP4 was selected due to the greater stability of the reductase *versus* AgcB from RHA1. AgcAB, VanAB, and PbdA/HaPuXR catalyze the *O*-demethylation of ethylguaiacol (**1a**), *p*-methoxybenzoate (**2a**), and vanillate (**3a**), to ethylcatechol (**1b**), hydroxybenzoate (**2b**), and protocatechuate (**3b**), respectively (Fig. 2A). To overcome the constraints of supplying stoichiometric NADH, we explored the use of SH from *C. necator* to efficiently regenerate $NAD^+$ using $H_2$ as the reductant.

We first investigated the effect of gas composition on reaction performance. Specifically, we assessed the minimum $H_2$ concentration required to sustain full turnover under constant $O_2$ (20%) and whether efficient operation could be achieved under non-explosive conditions. In 1 mL reactions performed in 8 mL gas tight vials, all three enzyme systems, AgcAB for the conversion of **1a** to **1b**, PbdA/HaPuXR for **2a** to **2b**, and VanAB for **3a** to **3b**, reached >99% substrate conversion when operated at $H_2$ concentrations of 4% or higher (SI Fig. S4). This corresponds to 13.6 μmol of $H_2$, slightly exceeding the 10 μmol of aromatic substrate in solution. At 2% $H_2$ (~6.8 μmol), conversions dropped sharply to ~60% across the three systems, consistent with a stoichiometric relationship between $H_2$ and product formation. This highlights the role of $H_2$ as a stoichiometric reagent under batch conditions. These results also establish that high enzymatic efficiency can be retained even at low $H_2$ partial pressures, consistent with SH's low $K_M$ value for $H_2$ (<40 μM) and highlighting the system's intrinsic safety and scalability.[58] Compared to previously reported $H_2$-driven biocatalytic processes, such as processes involving imine reductases (IREDs) and putrescine oxidases under 50 : 50 $H_2 : O_2$ ratios, IREDs at 100% $H_2$, or flavin-dependent oxidoreductases operating with 10% $O_2$ and 60% $H_2$, our system achieves complete substrate conversion using just 4% $H_2$ under atmospheric pressure conditions.[43,44,59] This positions our platform as a significant advancement in the safe operation of $H_2$-driven biocatalytic systems.

Moreover, the ~90% match between expected and observed conversion efficiencies under optimized conditions indicates that electron transfer from $H_2$ to the final product is relatively well-coupled. Each mole of $H_2$ donates two electrons, which are transferred *via* SH to $NAD^+$ and ultimately to the oxygenase through the reductase. Electrons may be lost to $O_2$ during this process, from either the reductase or the oxygenase, generating ROS. The two-component systems VanAB and AgcAB are well-coupled under certain conditions, as demonstrated previously for VanAB[34] and for AgcAB in unpublished data by Wolf *et al.* As the coupling of PbdA to HaPuXR was not known, we tested coupling with varying proportions of the three components. In these studies, a 10 : 5 : 1 ratio of PbdA : HaPuX : HaPuR maximized activity and coupling, and was used in subsequent experiments (SI Table S3). Overall, the relatively tight coupling from $H_2$ to final product reflects minimal loss of electrons throughout the electron transport chain.

We next examined the influence of $NAD^+$ concentration on each system's performance. Reactions were conducted with $NAD^+$ ranging from 0.1 to 0.4 mM, while maintaining 10 mM substrate and 4% $H_2$. As summarized in Fig. 2C, VanAB (**3a** to **3b**) demonstrated the most robust profile, with full conversion being achieved using 0.2 mM $NAD^+$. Reaction Mass Efficiency (RME) values remained consistently around 21%, indicating that the system performs well even under cofactor-limited conditions, with no gain in atom efficiency above 0.2 mM $NAD^+$ (SI Table S4). VanAB's high RME at lower $NAD^+$ concentration is comparable to those of conventional chemical processes for lignin valorization but is achieved under significantly milder conditions, enabling efficient substrate conversion with minimal waste.[60] AgcAB (**1a** to **1b**) required higher cofactor concentrations for stochiometric conversion ([$NAD^+$] = 0.3 mM). Finally, the three-component system PbdA/HaPuXR (**2a** to **2b**) showed lower relative performance. At 0.1 mM $NAD^+$, $TTN_{Ox}$ reached only 568, yielding 5.7 mM product with an RME of 15.9%. The reductase HaPuR was supplied at a 10-fold lower concentration than PbdA to maintain high coupling (SI

Open Access Article. Published on 08 December 2025. Downloaded on 1/7/2026 10:12:59 AM.
This article is licensed under a Creative Commons Attribution 3.0 Unported Licence.

Table S3) and likely restricted the comparative efficiency of this system.

Interestingly, AgcB and VanB have low $K_M$ values (12 and 10 μM, respectively) and high $k_{cat}/K_M$ values (1.3 and 3.0 $\mu M^{-1}$ $s^{-1}$, respectively) for NADH.[27,61] These high efficiencies support fast turnover at relatively low cofactor concentrations, consistent with the high TTN and RME values. Conversely, the $K_M$ of SH for $NAD^+$ is approximately 0.5 mM, which is slightly above the maximum tested concentration (0.4 mM). Under these conditions, $NAD^+$ concentration is not saturated for SH, resulting in sub-maximum reaction rates. Finally, RME varies not only with cofactor input, but also with the interplay between enzyme efficiency, time, and turnover balance. Identifying the lowest $NAD^+$ concentration at which complete conversion occurs without compromising time or yield is critical for scaling. Higher concentrations of $NAD^+$ may increase the reaction rate, but lower RME and cost efficiency.

In this study, we tested each of the enzyme systems for activity on their preferred monoaromatic substrate, all of which are LDACs. However, lignin processing frequently produces higher order lignin-derived oligomers.[62] Although activity of AgcA, PbdA and VanA on lignin-derived oligomers has not been explored experimentally, it is unlikely to be significant given the enzymes' respective substrate specificities. We further note that emergent lignin valorization strategies seek to increase monomeric yields, a priority that aligns with a set-up involving monomer-active enzymes.[14,63]

By combining TTN, RME, and product yield, our data highlight how careful optimization of cofactor input across different catalytic architectures enables the development of $H_2$-driven systems that are not only effective, but also sustainable.

### Formaldehyde tolerance of the biocatalytic components

The enzymatic *O*-demethylation of LDACs results in the production of formaldehyde (Fig. 2A).[64,65] In light of formaldehyde's ability to inactivate enzymes,[37,66] we assessed the formaldehyde tolerance of the different components of our $H_2$-driven systems. More specifically, we evaluated the relative activities of AgcAB, PbdA/HaPuXR, and VanAB across 0–40 mM formaldehyde (Fig. 3). At the lowest formaldehyde concentration (2.5 mM), all three systems retained over 90% of their initial activity, indicating a tolerance to low concentrations of small aldehydes. However, with increasing formaldehyde concentrations, significant differences in activity attenuation were observed among the systems. VanAB exhibited the highest tolerance, retaining approximately 90% of its initial activity at 5 mM formaldehyde, and maintained around 40% activity at 20 mM. In contrast, AgcAB and PbdA/HaPuXR were more sensitive, with both systems exhibiting ~70% and ~40% activity at 5 and 10 mM formaldehyde, respectively.

We also assessed the activities of two NADH regeneration enzymes, SH and the commercial *C. boidinii* metal-independent FDH (Fig. 3B). SH exhibited remarkable tolerance, maintaining over 85% activity at 5 mM formaldehyde and retaining over 50% activity at 20 mM. In comparison, the activity of FDH

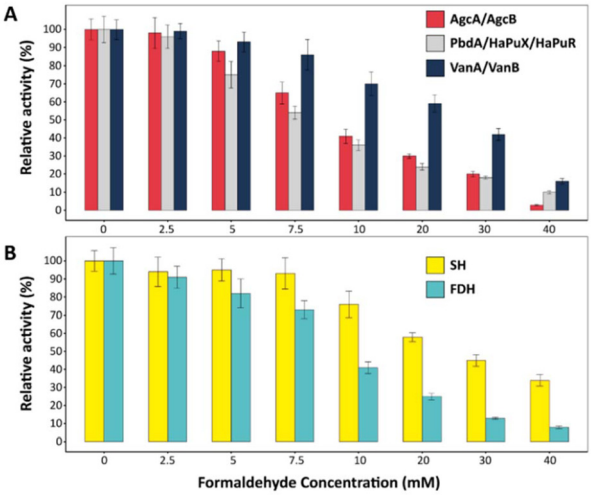


**Fig. 3** Differential formaldehyde sensitivity of oxygenases and $NAD^+$ reducing modules. (A) The figure illustrates the formaldehyde tolerance of the three oxidoreductase systems AgcA/AgcB, PbdA/HaPuX/HaPuR, and VanA/VanB, expressed as the relative NADH oxidation activity (%) at increasing formaldehyde concentrations (0–40 mM). Reactions were performed in 2 mL quartz cuvettes, enzyme concentrations were 5 μM for AgcA/AgcB, 10 μM for VanA/VanB, 10 μM for PbdA, 5 μM for HaPuX, and 1 μM for HaPuR, with 0.4 mM NADH as the electron donor. (B) Relative activity of the NADH regeneration systems SH (soluble [NiFe]-hydrogenase) and FDH (formate dehydrogenase) under identical conditions. Both systems catalyze the reduction of $NAD^+$ to NADH, with SH using $H_2$ as electron donor and FDH using formate. Enzyme concentrations were 2.5 μM for SH and 3 U $mL^{-1}$ for FDH, with 0.4 mM $NAD^+$. *T*-Tests revealed that SH maintained significantly higher activity compared to FDH at formaldehyde concentrations ≥5 mM ($p < 0.05$), with pronounced significance at ≥20 mM ($p < 0.005$).

sharply declined, with more than 50% inhibition observed at 10 mM formaldehyde, and less than 20% activity at concentrations above 20 mM.

Without further study, it is unclear why VanAB is more formaldehyde-tolerant than AgcAB and PbdA/HaPuXR, or whether this property reflects ROs and P450s more broadly. Regarding the cofactor regeneration systems, the remarkable tolerance of SH may be due to its FeS cluster-based mechanism for electron transfer from the NiFe site, which minimizes susceptibility to electrophilic modifications. In contrast, FDH catalyzes direct hydride transfer from formate to $NAD^+$ and relies on cysteine residues for activity. These thiol groups are highly reactive toward electrophiles such as formaldehyde, making FDH more susceptible to formaldehyde-induced inactivation.[67] This observed difference in formaldehyde tolerance is consistent with previous comparative studies on [FeFe]- and [NiFe]-hydrogenases, which provide valuable insights into how redox-active metal centers interact with formaldehydes.[68] Furthermore, the [NiFe]- active site, in contrast to metal-independent FDHs, is deeply buried within the enzyme, with access controlled by a gas tunnel that limits formaldehyde entry.[69] This structural feature provides an additional protective mechanism, preventing small reactive species like formaldehyde from directly modifying the metal center.[68] This struc-

Open Access Article. Published on 08 December 2025. Downloaded on 1/7/2026 10:12:59 AM.
This article is licensed under a Creative Commons Attribution 3.0 Unported Licence.

tural advantage makes the SH more suitable for applications involving aldehyde-generating biotransformations. When compared to other NADH regeneration systems such as FDH, SH offers a unique advantage in formaldehyde-rich environments while also minimizing byproduct formation. Despite the retained activity of both the oxidoreductase systems and SH, formaldehyde accumulation during lignin valorization remains a critical challenge in setups that involve a higher substrate load.

### Electro-driven *O*-demethylation with closed-loop flow biocatalysis

To enable continuous formaldehyde removal, scale-up, and *in situ* $H_2$ supply, we designed a closed-loop flow biocatalysis system. Due to its higher formaldehyde tolerance compared to the other two *O*-demethylase systems, VanAB was assessed in the flow system. Our initial attempts to immobilize VanAB using metal ion affinity beads (EziG) resulted in complete loss of activity, likely due to disruption of the direct interaction between the two components that is required for electron transfer. To address this, a closed-loop flow system was developed with a dialysis membrane (MWCO 3.5 kDa) that entrapped VanAB in a 5 mL volume, referred to here as the biotransformation unit.[70,71] This maintained the two components at relatively high concentrations, maximizing their interaction and therefore activity. SH was immobilized on Amberlite FPA.[54] an anionic resin, enabling $H_2$-driven NADH regeneration. To introduce $H_2$ and $O_2$ continuously to the bioreactor in the correct proportions, separate gas addition modules were implemented to reduce gas competition due to differential solubility and diffusion rates (Fig. 4A). The $H_2$ module was positioned in the flow sequence directly upstream of the $O_2$ module. This arrangement ensured accurate tuning of the gas composition without direct aeration into the reaction volume avoiding inactivation by shear force. Using $H_2$ and $O_2$ from water electrolysis, SH-Amberlite facilitated reduction of $NAD^+$ for VanAB even at 15% $O_2$ (Fig. 4C).

The entrapped VanAB in the biotransformation unit exhibited high activity, converting >99% of 50 mM vanillate (**3a**) to protocatechuate (**3b**) within 5 h (Fig. 4B). The biotransformation unit was maintained at 30 °C using a heating panel to enhance VanAB activity. The formation of reactive oxygen species was prevented by adding catalase to the biotransformation unit. The biotransformation unit was open to the atmosphere allowing equilibration with air. This presumably helped keep formaldehyde concentration below 0.5 mM (Fig. 4B). Finally, since the enzymes were immobilized on columns/within the biotransformation unit, the flow volume only contained **3a**/**3b** and $NAD^+$/NADH. This design greatly facilitated a simple product extraction using diethyl ether, where the 200 mL reaction volume yielded 1.542 g (95% isolated yield) of protocatechuate (**3b**).

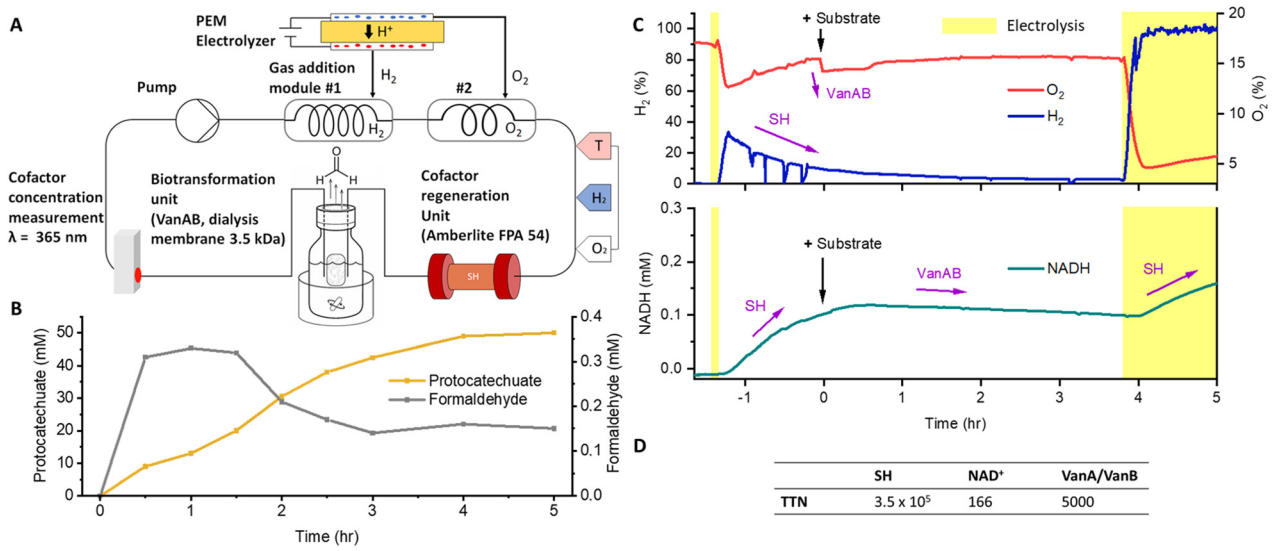


| | SH | NAD+ | VanA/VanB |
|---|---|---|---|
| TTN | 3.5 x 10^5 | 166 | 5000 |

**Fig. 4** Integrated flow system for electrolysis-powered biocatalytic *O*-demethylation of vanillate. (A) Flow setup for electro-driven *O*-demethylation of vanillate. $H_2$ is produced from a PEM electrolyzer using $Pt_B/Pt_C$ as a $H_2$ evolution catalyst. Two gas addition modules are used to transfer $H_2$ and $O_2$ to the 200 mL closed-loop system containing 20 mM Tris-HCl buffer (pH 8.0), 50 mM vanillate (**3a**) and 0.3 mM $NAD^+$. $H_2$, $O_2$, and temperature sensors together with a spectrophotometer were integrated. 1 mg of SH was immobilized by Amberlite FPA. VanA and VanB were entrapped in a dialysis membrane and integrated as a biotransformation unit. (B) Product protocatechuate yield (dark yellow) and formaldehyde concentration (dark gray) across time points during the upscaled reaction of electro/−$H_2$ driven O-demethylation of vanillate. (C) On-line monitoring of $H_2$, $O_2$ (up), and NADH (down) during the electro-driven biotransformation. The concentration of $H_2$ (blue), $O_2$ (red), and NADH (green) were followed during the time of reaction. The pulsed electrolysis is also depicted (yellow box). $NAD^+$ was added before the electrolysis, then substrate was added after NADH reached a plateau. After 3.8 hours substrate addition, $H_2$ and $O_2$ were supplied again with a lower rate. Purple arrows indicate the activity of each enzyme. (D) Total turnover numbers of all biocatalysts ($n_{product}/n_{enzyme}$) and cofactors ($n_{product}/n_{NAD^+}$) involved in the closed-loop flow setup process.

Open Access Article. Published on 08 December 2025. Downloaded on 1/7/2026 10:12:59 AM.
This article is licensed under a Creative Commons Attribution 3.0 Unported Licence.

The described flow system can be compared to fed-batch fermentation using VanAB-expressing *P. putida*, where equimolar formaldehyde during the *O*-demethylation reaction limits protocatechuate production to 17.5 g $L^{-1}$ in 50 mL media.[72] In contrast, the flow setup enables continuous removal of formaldehyde and offers modular scalability by connecting or expanding reactor units, providing a directly controllable operational format. For gas-dependent transformations, scale-up limitations in gas-to-liquid transfer can be alleviated by extending the gas-permeable tubing within the gas addition module, thereby improving mass transfer. In the flow reaction, the TTN of SH and VanAB reached up to 3.5 × $10^5$ and 5000, respectively, showing high stability of the enzymes (Fig. 4D). The high $TTN_{SH}$ compared to the batch reactions is due to a lower enzyme load and an increased product yield. The $TTN_{SH}$ in our upscaled flow reactions is more than three-fold higher than that of a comparable system for flavin-dependent biocatalysis, where the SH was immobilized on Strep-Tactin XT resin.[42] This high TTN for SH-Amberlite corroborates previous reports, where Amberlite FPA[54] served as a stable enzyme carrier for SH reaching TTN values of up to 1.1 × $10^6$ after six cycles.[41] The TTN of entrapped VanAB was three-fold higher than that reported for other RO systems, including a sophisticated hybrid system comprising cumene dioxygenase and the reductase from phthalate dioxygenase (TTN of 1515).[73] This illustrates the challenges of the redox interactions in ROs and also demonstrates that they can be effectively stabilized through entrapment for flow applications.

Prior studies applied PVDF (polyvinylidene fluoride) membranes as teabags, entrapping lyophilized whole-cell biocatalysts for stereoselective synthesis.[70] Similar catalyst containment using dialysis membranes such as PVDF has been used since the 1980s as drug-delivery systems and, more recently, for oxazoline Cu(II) Lewis acid catalysts.[71,74] Dialysis membranes offer molecular weight cut-off control, ease of handling, and robust structural integrity under various pH/temperature conditions compared to other entrapment methods such as hydrogels.[75] Also, enzyme entrapment applications serve as an excellent alternative to enzymatic membrane reactors (EMRs), ensuring efficient diffusion, reusability of the enzymes. Finally, entrapment does not require high-pressure systems and maintains enzyme stability. Overall, the high $TTN_{VanAB}$ achieved here establishes that entrapment with dialysis membrane is a viable method for stabilizing multi-component oxidoreductases in flow systems.

To facilitate optimization of the bioreactor, we monitored various parameters online during the reaction, including the electrocatalytic evolution of the gases and their enzymatic consumption (Fig. 4C). Faradaic efficiency was improved by pulsing the PEM electrolysis. After 5 min of electrolysis (3.9 V, 2.21 A), 25% dissolved $H_2$ and 12% dissolved $O_2$ were reached in the flow system (Fig. 4C). At 3.8 h after the addition of substrate, the electrolysis was activated again (3.5 V, 1.03 A) for 1.2 h to further increase the reaction rate. A sharp decrease in dissolved $O_2$ concentration upon substrate addition was observed, indicating $O_2$ consumption by VanAB during *O*-demethylation. In the flow setup, the spectrophotometer for monitoring NADH was positioned downstream of the biotransformation unit. As a result, the detected NADH concentration reflected its level post-enzymatic consumption. Four hours after substrate addition, an increase of NADH concentration was observed, indicating the completion of VanAB reaction. This was confirmed by GC (Fig. 4B) and online TLC monitoring. The higher NADH concentration may also reflect increased SH activity due to higher $H_2$ concentrations from water electrolysis (Fig. 4C).

We also determined the faradaic efficiency for the electro-driven *O*-demethylation of **3a** to **3b** in the flow system. Five hours after substrate addition, with 99% conversion, the faradaic efficiency of the flow system was 18% (SI section S4). However, the electron contribution to product formation was three-fold higher (62%) when measured to 4 h after substrate addition. At that timepoint, only 12 min of electrolysis was performed, despite near-complete vanillate turnover. The lower faradaic efficiency observed at 5 h suggests that during prolonged operation, a significant portion of electrons supplied during electrolysis no longer contributes to product formation. This may reflect mostly complete substrate conversion, although the open biotransformation unit must result in $H_2$ loss and thus lowered efficiency. The high faradaic efficiency relative to substrate conversion in this system suggests that only 5–10 min of electrolysis is sufficient to drive the reaction in the flow system. The faradaic efficiency of bioelectrocatalytic systems can reach up to 100% when electron transfer from the electrode to the enzymes is directly and optimally controlled.[76] Nevertheless, the 62% faradaic efficiency achieved with the current design is over 400-fold higher than that reported for another closed-loop biocatalytic flow setup.[42] While high atom efficiency and faradaic efficiency were demonstrated in this system, optimizing the balance between reaction time with electrolysis duration is critical to further optimizing the process's energy efficiency. We evaluated waste production using the environmental factor (*E*-factor).[79,80] For the 200 mL reaction performed here, the *E*-factor was 3.6 and the $E^+$-factor was 2850 (Table 1 and SI Table S6). This indicates that less waste was formed than in conventional NADH regeneration systems used other oxidoreductase reactions.[77–80] For instance, glucose/GDH-based regeneration produces stoichiometric quantities of gluconolactone or gluconic acid as waste products. In contrast, $H_2$-driven regeneration using SH generates

**Table 1** Environmental and biocatalytic parameters of flow system for vanillate conversion

| Parameters | Values |
|---|---|
| *E*-Factor | 3.6 |
| $E^+$-Factor | 2850 |
| EcoScale | 88 |
| Carbon efficiency | 87.5% |
| Atom efficiency | 76.2% |
| RME | 90.3% |

Open Access Article. Published on 08 December 2025. Downloaded on 1/7/2026 10:12:59 AM.
This article is licensed under a Creative Commons Attribution 3.0 Unported Licence.

no organic byproducts. This is reflected in high EcoScale atom and carbon efficiencies (Table 1). Overall, the $H_2$/electro-driven biocatalytic *O*-demethylation process demonstrates significantly lower waste generation than previously reported electro-biocatalytic approaches. Reuse of the nicotinamide cofactor offers an effective route to increase the operational TTN. NAD(H) can be retained or recaptured during product isolation using established separation strategies such as membrane processes that exploit size and Donnan exclusion.[81] Cofactor immobilization on functionalized polymers or silica supports is another option, though typically accompanied by diffusional limitations, reduced turnover, and higher material costs.[82] These constraints should be carefully considered when evaluating immobilization for continuous operation. As an outlook, the demethylated carboxylates could be recovered using established aqueous-phase separations, including pH-shift liquid–liquid extraction, capture and release on anion-exchange or polymeric adsorption resins (with optional in-flow product removal).[83]

## Conclusions

This study presents a scalable, energy-efficient biocatalytic system for valorizing LDACs. More specifically, our bioreactor for electro-driven *O*-demethylation integrates water electrolysis with $H_2$-driven NADH regeneration and a simple entrapment system for multicomponent oxygenases. We optimized the activity of three such oxygenases, AgcAB, PbdA/HaPuXR, and VanAB, with the $H_2$/SH cofactor regeneration system, demonstrating the feasibility of using these enzymes at low concentrations of $H_2$ and $NAD^+$ while maintaining tolerance to formaldehyde. The closed-loop flow system achieved scalable and optimized electro-driven biocatalytic *O*-demethylation. Using VanAB for proof-of-concept, we established a flow system that can valorize LDACs in high atom efficiency. In future, the system could be further refined to support continuous product release by integration of an *in situ* product extraction module and optimized by scalable gas transfer. The inclusion of gas sensors within the setup also allowed real-time monitoring of the interplay between water electrolysis and biocatalysis, providing valuable insight for future process development. This platform allowed for the implementation of pulsed electrolysis and improved faradaic efficiency, as well as ensuring safe and scalable biotransformation. Importantly, the described platform provides a foundation for broader applications involving NAD(P)H-utilizing multicomponent oxidoreductases systems such as soluble methane monooxygenase as well as other P450s and ROs. Looking ahead, future scale-up should focus on integrating a low-temperature in-line capture unit to condense and retain evaporated formaldehyde, thereby enabling its selective removal and continuous recovery. Such a capture stream creates opportunities for sustainable valorization: recovered formaldehyde can be converted into chiral amines *via* IRED-catalyzed reductive amination,[84] or transformed into higher carbon products through formolase-mediated C–C bond formation.[85] In parallel, further optimization of electrolysis parameters, combined with cofactor immobilization or entrapment, is expected to enhance process robustness and long-term operation. These improvements may also expand compatibility with alternative reaction media, including organic solvents and deep eutectic systems,[86] thereby offering expanded possibilities for future green biotransformations.

## Author contributions

L. L., D. C., and G. L. conceptualized the study; D. C., G. L., P. N., and M. E. W. designed and conducted the experiments; D. C. and G. L. performed the formal analysis; L. L. secured funding for the project; L. L., P. R. F. C., and L. E. supervised the research and provided guidance throughout the study; D. C. and G. L. prepared the original manuscript draft; L. L., P. R. F. C., L. E., D. C., and G. L. reviewed and edited the manuscript; all authors contributed to data analysis and discussions.

## Conflicts of interest

There are no conflicts to declare.

## Data availability

The data supporting this article have been included as part of the supplementary information (SI). Supplementary information is available. See DOI: https://doi.org/10.1039/d5gc05054e.

Raw and metadata for this contribution are available at https://doi.org/10.5281/zenodo.14604224.

## Acknowledgements

This project received funding from the European Union's Horizon 2020 research and innovation programme under the Marie Skłodowska-Curie grant agreement No. 955740, from the Deutsche Forschungsgemeinschaft (DFG, German Research Foundation) under Germany's Excellence Strategy—Cluster of Excellence 2186 "The Fuel Science Center" (ID: 390919832), by the Werner Siemens Foundation (WSS) through the Forschungszentrum catalaix, from the LignoPharm project within the Bioeconomy Science Center (BioSC, No. 005-2012-0107), supported by the Ministry of Culture and Science of the State of North Rhine-Westphalia, as well as the Natural Sciences and Engineering Research Council of Canada (DG 171359) to L. D. E. M. E. W. is the recipient of a Canada Graduate Scholarship-Doctoral. We thank Dr. Meike Emondts (ITMC, DWI–RWTH Aachen University) for her support with NMR spectroscopy, including both instrument access and assistance with data analysis.

Open Access Article. Published on 08 December 2025. Downloaded on 1/7/2026 10:12:59 AM.
This article is licensed under a Creative Commons Attribution 3.0 Unported Licence.

## References

1 R. Rinaldi, R. Jastrzebski, M. T. Clough, J. Ralph, M. Kennema, P. C. A. Bruijnincx and B. M. Weckhuysen, Paving the Way for Lignin Valorisation: Recent Advances in Bioengineering, Biorefining and Catalysis, *Angew. Chem., Int. Ed.*, 2016, **55**, 8164–8215.

2 J. J. Del Río, J. Rencoret, A. Gutiérrez, T. Elder, H. Kim and J. Ralph, Lignin Monomers from beyond the Canonical Monolignol Biosynthetic Pathway: Another Brick in the Wall, *ACS Sustainable Chem. Eng.*, 2020, **8**(13), 4997–5012.

3 A. J. Ragauskas, G. T. Beckham, M. J. Biddy, R. Chandra, F. Chen, M. F. Davis, B. H. Davison, R. A. Dixon, P. Gilna, M. Keller, P. Langan, A. K. Naskar, J. N. Saddler, T. J. Tschaplinski, G. A. Tuskan and C. E. Wyman, Lignin valorization: Improving lignin processing in the biorefinery, *Science*, 2014, **344**, 1246843.

4 W. Schutyser, T. Renders, S. Van Den Bosch, S. F. Koelewijn, G. T. Beckham and B. F. Sels, Chemicals from lignin: an interplay of lignocellulose fractionation, depolymerisation, and upgrading, *Chem. Soc. Rev.*, 2018, **47**, 852–908.

5 Z. Sun, B. Fridrich, A. De Santi, S. Elangovan and K. Barta, Bright Side of Lignin Depolymerization: Toward New Platform Chemicals, *Chem. Rev.*, 2018, **118**, 614–678.

6 J. Zakzeski, P. C. A. Bruijnincx, A. L. Jongerius and B. M. Weckhuysen, The catalytic valorization of lignin for the production of renewable chemicals, *Chem. Rev.*, 2010, **110**, 3552–3599.

7 M. M. Abu-Omar, K. Barta, G. T. Beckham, J. S. Luterbacher, J. Ralph, R. Rinaldi, Y. Román-Leshkov, J. S. M. Samec, B. F. Sels and F. Wang, Guidelines for performing lignin-first biorefining, *Energy Environ. Sci.*, 2021, **14**, 262–292.

8 G. T. Beckham, C. W. Johnson, E. M. Karp, D. Salvachúa and D. R. Vardon, Opportunities and challenges in biological lignin valorization, *Curr. Opin. Biotechnol*, 2016, **42**, 40–53.

9 S. Shrestha, S. Goswami, D. Banerjee, V. Garcia, E. Zhou, C. N. Olmsted, E. L. W. Majumder, D. Kumar, D. Awasthi, A. Mukhopadhyay, S. W. Singer, J. M. Gladden, B. A. Simmons and H. Choudhary, Perspective on Lignin Conversion Strategies That Enable Next Generation Biorefineries, *ChemSusChem*, 2024, **17**, e202301460.

10 L. D. Eltis and R. Singh, Biological Funneling as a Means of Transforming Lignin-derived Aromatic Compounds into Value-added Chemicals, *RSC Energy Environ. Ser.*, 2018, 290–313.

11 E. M. Anderson, R. Katahira, M. Reed, M. G. Resch, E. M. Karp, G. T. Beckham and Y. Román-Leshkov, Reductive Catalytic Fractionation of Corn Stover Lignin, *ACS Sustainable Chem. Eng.*, 2016, **4**, 6940–6950.

12 Y. Liao, S. F. Koelewijn, G. van den Bossche, J. van Aelst, S. van den Bosch, T. Renders, K. Navare, T. Nicolaï, K. van Aelst, M. Maesen, H. Matsushima, J. M. Thevelein, K. van Acker, B. Lagrain, D. Verboekend and B. F. Sels, A sustainable wood biorefinery for low-carbon footprint chemicals production, *Science*, 2020, **367**, 1385–1390.

13 S. Van Den Bosch, W. Schutyser, R. Vanholme, T. Driessen, S. F. Koelewijn, T. Renders, B. De Meester, W. J. J. Huijgen, W. Dehaen, C. M. Courtin, B. Lagrain, W. Boerjan and B. F. Sels, Reductive lignocellulose fractionation into soluble lignin-derived phenolic monomers and dimers and processable carbohydrate pulps, *Energy Environ. Sci.*, 2015, **8**, 1748–1763.

14 C. T. Palumbo, N. X. Gu, A. C. Bleem, K. P. Sullivan, R. Katahira, L. M. Stanley, J. K. Kenny, M. A. Ingraham, K. J. Ramirez, S. J. Haugen, C. R. Amendola, S. S. Stahl and G. T. Beckham, Catalytic carbon–carbon bond cleavage in lignin via manganese–zirconium-mediated autoxidation, *Nat. Commun.*, 2024, **15**, 1–12.

15 J. G. Tillou, C. J. Ezeorah, J. J. Kuchta, S. C. D. D. Mudiyanselage, J. D. Sitter and A. K. Vannucci, A review on recent trends in selective hydrodeoxygenation of lignin derived molecules, *RSC Sustainability*, 2023, **1**, 1608–1633.

16 Y. Wang, M. Chen, Y. Yang, J. Ralph and X. Pan, Efficient O-Demethylation of lignin-derived aromatic compounds under moderate conditions, *RSC Adv.*, 2023, **13**, 5925–5932.

17 S. B. Waghmode, G. Mahale, V. P. Patil, K. Renalson and D. Singh, Efficient Method for Demethylation of Aryl Methyl Ether Using Aliquat-336, *Synth. Commun.*, 2013, **43**, 3272–3280.

18 K. Hwang and S. Park, Selective Cleavage of Aryl Methyl Ether Moiety of Aryloxy Aryl Methyl Ether by 48% Hbr/Tetra-n-butylphosphonium Bromide, *Synth. Commun.*, 1993, **23**, 2845–2849.

19 X. Li, J. He and Y. Zhang, BBr3-Assisted Preparation of Aromatic Alkyl Bromides from Lignin and Lignin Model Compounds, *J. Org. Chem.*, 2018, **83**, 11019–11027.

20 E. Grabińska-Sota and J. Kalka, An assessment of the toxicity of pyridinium chlorides and their biodegradation intermediates, *Environ. Int.*, 2003, **28**, 687–690.

21 D. Sang, X. Tu, J. Tian, Z. He and M. Yao, Anchimerically Assisted Cleavage of Aryl Methyl Ethers by Aluminum Chloride-Sodium Iodide in Acetonitrile, *ChemistrySelect*, 2018, **3**, 10103–10107.

22 F. Lin, M. Xu, K. K. Ramasamy, Z. Li, J. L. Klinger, J. A. Schaidle and H. Wang, Catalyst Deactivation and Its Mitigation during Catalytic Conversions of Biomass, *ACS Catal.*, 2022, **12**, 13555–13599.

23 E. Erickson, A. Bleem, E. Kuatsjah, A. Z. Werner, J. L. DuBois, J. E. McGeehan, L. D. Eltis and G. T. Beckham, Critical enzyme reactions in aromatic catabolism for microbial lignin conversion, *Nat. Catal.*, 2022, **5**, 86–98.

24 M. E. Wolf, D. J. Hinchen, J. E. McGeehan and L. D. Eltis, Characterization of a cytochrome P450 that catalyzes the *O*-demethylation of lignin-derived benzoates, *J. Biol. Chem.*, 2024, **300**, 107809.

25 H. P. Chen, M. Chow, C. C. Liu, A. Lau, J. Liu and L. D. Eltis, Vanillin catabolism in *Rhodococcus jostii* RHA1, *Appl. Environ. Microbiol.*, 2012, **78**, 586–588.

Open Access Article. Published on 08 December 2025. Downloaded on 1/7/2026 10:12:59 AM.
This article is licensed under a Creative Commons Attribution 3.0 Unported Licence.

26 M. E. Wolf, D. J. Hinchen, J. L. DuBois, J. E. McGeehan and L. D. Eltis, Cytochromes P450 in the biocatalytic valorization of lignin, *Curr. Opin. Biotechnol*, 2022, **73**, 43–50.

27 M. M. Fetherolf, D. J. Levy-Booth, L. E. Navas, J. Liu, J. C. Grigg, A. Wilson, R. Katahira, G. T. Beckham, W. W. Mohn and L. D. Eltis, Characterization of alkylguaiacol-degrading cytochromes P450 for the biocatalytic valorization of lignin, *Proc. Natl. Acad. Sci. U. S. A.*, 2020, **117**, 25771–25778.

28 F. F. Özgen and S. Schmidt, Rieske non-heme iron dioxygenases: Applications and future perspectives, in *Biocatalysis: Enzymatic Basics and Applications*, 2019, pp. 57–82.

29 J. García-Hidalgo, K. Ravi, L. L. Kuré, G. Lidén and M. Gorwa-Grauslund, Identification of the two-component guaiacol demethylase system from *Rhodococcus rhodochrous* and expression in *Pseudomonas putida* EM42 for guaiacol assimilation, *AMB Express*, 2019, **9**, 34.

30 A. C. Harlington, T. Das, K. E. Shearwin, S. G. Bell and F. Whelan, Structural insights into S-lignin O-demethylation via a rare class of heme peroxygenase enzymes, *Nat. Commun.*, 2025, **16**, 1815.

31 T. Sonoki, T. Obi, S. Kubota, M. Higashi, E. Masai and Y. Katayama, Coexistence of two different *O* demethylation systems in lignin metabolism by *Sphingomonas paucimobilis* SYK-6: Cloning and sequencing of the lignin biphenyl-specific *O*-demethylase (LigX) gene, *Appl. Environ. Microbiol.*, 2000, **66**, 2125–2132.

32 A. Bleem, E. Kuatsjah, G. N. Presley, D. J. Hinchen, M. Zahn, D. C. Garcia, W. E. Michener, G. König, K. Tornesakis, M. N. Allemann, R. J. Giannone, J. E. McGeehan, G. T. Beckham and J. K. Michener, Discovery, characterization, and metabolic engineering of Rieske non-heme iron monooxygenases for guaiacol *O*-demethylation, *Chem. Catal.*, 2022, **2**, 1989–2011.

33 S. J. B. Mallinson, M. M. Machovina, R. L. Silveira, M. Garcia-Borràs, N. Gallup, C. W. Johnson, M. D. Allen, M. S. Skaf, M. F. Crowley, E. L. Neidle, K. N. Houk, G. T. Beckham, J. L. Dubois and J. E. McGeehan, A promiscuous cytochrome P450 aromatic O-demethylase for lignin bioconversion, *Nat. Commun.*, 2018, **9**, 1–12.

34 S. Notonier, A. Z. Werner, E. Kuatsjah, L. Dumalo, P. E. Abraham, E. A. Hatmaker, C. B. Hoyt, A. Amore, K. J. Ramirez, S. P. Woodworth, D. M. Klingeman, R. J. Giannone, A. M. Guss, R. L. Hettich, L. D. Eltis, C. W. Johnson and G. T. Beckham, Metabolism of syringyl lignin-derived compounds in *Pseudomonas putida* enables convergent production of 2-pyrone-4,6-dicarboxylic acid, *Metab. Eng.*, 2021, **65**, 111–122.

35 F. Brunel and J. Davison, Cloning and sequencing of Pseudomonas genes encoding vanillate demethylase, *J. Bacteriol.*, 1988, **170**, 4924–4930.

36 D. French and J. T. Edsall, The Reactions of Formaldehyde with Amino Acids and Proteins, *Adv. Protein. Chem.*, 1945, **2**, 277–335.

37 B. Metz, G. F. A. Kersten, G. J. E. Baart, A. De Jong, H. Meiring, J. ten Hove, M. J. Van Steenbergen, W. E. Hennink, D. J. A. Crommelin and W. Jiskoot, Identification of formaldehyde-induced modifications in proteins: Reactions with insulin, *Bioconjugate Chem.*, 2006, **17**, 815–822.

38 S. Mordhorst and J. N. Andexer, Round, round we go – strategies for enzymatic cofactor regeneration, *Nat. Prod. Rep.*, 2020, **37**, 1316–1333.

39 W. Liu and P. Wang, Cofactor regeneration for sustainable enzymatic biosynthesis, *Biotechnol. Adv.*, 2007, **25**, 369–384.

40 K. Bachosz, J. Zdarta, M. Bilal, A. S. Meyer and T. Jesionowski, Enzymatic cofactor regeneration systems: A new perspective on efficiency assessment, *Sci. Total Environ.*, 2023, **868**, 161630.

41 A. Al-Shameri, M.-C. Petrich, K. junge Puring, U.-P. Apfel, B. M. Nestl and L. Lauterbach, Powering Artificial Enzymatic Cascades with Electrical Energy, *Angew. Chem., Int. Ed.*, 2020, **59**, 10929–10933.

42 G. Lim, D. Calabrese, A. Wolder, P. R. F. Cordero, D. Rother, F. F. Mulks, C. E. Paul and L. Lauterbach, $H_2$-driven biocatalysis for flavin-dependent ene-reduction in a continuous closed-loop flow system utilizing $H_2$ from water electrolysis, *Commun. Chem.*, 2024, **7**, 1–7.

43 A. Al-Shameri, S. J. P. Willot, C. E. Paul, F. Hollmann and L. Lauterbach, $H_2$ as a fuel for flavin- and $H_2O_2$-dependent biocatalytic reactions, *Chem. Commun.*, 2020, **56**, 9667–9670.

44 N. Borlinghaus, D. Calabrese, L. Lauterbach and B. M. Nestl, Synthesis of Substituted Acyclic and Cyclic N-Alkylhydrazines by Enzymatic Reductive Hydrazinations, *ChemBioChem*, 2024, e202400700.

45 H. A. Reeve, L. Lauterbach, P. A. Ash, O. Lenz and K. A. Vincent, A modular system for regeneration of NAD cofactors using graphite particles modified with hydrogenase and diaphorase moieties, *Chem. Commun.*, 2012, **48**, 1589–1591.

46 A. Al-Shameri, D. L. Siebert, S. Sutiono, L. Lauterbach and V. Sieber, Hydrogenase-based oxidative biocatalysis without oxygen, *Nat. Commun.*, 2023, **14**, 1–8.

47 L. Lauterbach and O. Lenz, How to make the reducing power of $H_2$ available for in vivo biosyntheses and biotransformations, *Curr. Opin. Chem. Biol.*, 2019, **49**, 91–96.

48 L. Lauterbach and O. Lenz, Catalytic production of hydrogen peroxide and water by oxygen-tolerant [NiFe]-hydrogenase during $H_2$ cycling in the presence of $O_2$, *J. Am. Chem. Soc.*, 2013, **135**, 17897–17905.

49 O. Lenz, M. Ludwig, T. Schubert, I. Bürstel, S. Ganskow, T. Goris, A. Schwarze and B. Friedrich, $H_2$ Conversion in the Presence of $O_2$ as Performed by the Membrane-Bound [NiFe]-Hydrogenase of *Ralstonia eutropha*, *ChemPhysChem*, 2010, **11**, 1107–1119.

50 L. Greiner, D. H. Müller, E. C. D. Van Den Ban, J. Wöltinger, C. Wandrey and A. Liese, Membrane Aerated Hydrogenation: Enzymatic and Chemical Homogeneous Catalysis, *Adv. Synth. Catal.*, 2003, **345**, 679–683.

Open Access Article. Published on 08 December 2025. Downloaded on 1/7/2026 10:12:59 AM.
This article is licensed under a Creative Commons Attribution 3.0 Unported Licence.

51 P. Schoenmakers, R. Rad, A. Ihl, I. Weickardt, S. Guillouet, U. P. Apfel and L. Lauterbach, Isopropanol production from carbon dioxide by *Cupriavidus necator* using a zero-gap cell with culture broth as catholyte, *iScience*, 2025, **28**, 113018.

52 R. Rad, T. Gehring, K. Pellumbi, D. Siegmund, E. Nettmann, M. Wichern and U. P. Apfel, A hybrid bioelectrochemical system coupling a zero-gap cell and a methanogenic reactor for carbon dioxide reduction using a wastewater-derived catholyte, *Cell Rep. Phys. Sci.*, 2023, **4**, 101526.

53 C. Liu, B. C. Colón, M. Ziesack, P. A. Silver and D. G. Nocera, Water splitting-biosynthetic system with $CO_2$ reduction efficiencies exceeding photosynthesis, *Science*, 2016, **352**(6290), 1210–1213.

54 J. Britton, S. Majumdar and G. A. Weiss, Continuous flow biocatalysis, *Chem. Soc. Rev.*, 2018, **47**, 5891–5918.

55 S. V. Ley, On Being Green: Can Flow Chemistry Help?, *Chem. Rec.*, 2012, **12**, 378–390.

56 L. E. Meyer, M. Hobisch and S. Kara, Process intensification in continuous flow biocatalysis by up and downstream processing strategies, *Curr. Opin. Biotechnol*, 2022, **78**, 102835.

57 M. A. Ramirez, S. Joseph Srinivasan, S. E. Cleary, P. M. T. Todd, H. A. Reeve and K. A. Vincent, $H_2$-Driven Reduction of Flavin by Hydrogenase Enables Cleaner Operation of Nitroreductases for Nitro-Group to Amine Reductions, *Front. Catal.*, 2022, **2**, 906694.

58 L. Lauterbach, O. Lenz and K. A. Vincent, $H_2$-driven cofactor regeneration with $NAD(P)^+$-reducing hydrogenases, *FEBS J.*, 2013, **280**, 3058–3068.

59 A. Al-Shameri, N. Borlinghaus, L. Weinmann, P. N. Scheller, B. M. Nestl and L. Lauterbach, Synthesis of N-heterocycles from diamines via $H_2$-driven NADPH recycling in the presence of $O_2$, *Green Chem.*, 2019, **21**, 1396–1400.

60 J. Park, M. A. Kelly, J. X. Kang, S. S. Seemakurti, J. L. Ramirez, M. C. Hatzell, C. Sievers and A. S. Bommarius, Production of active pharmaceutical ingredients (APIs) from lignin-derived phenol and catechol, *Green Chem.*, 2021, **23**, 7488–7498.

61 A. C. Bleem, E. Kuatsjah, J. Johnsen, E. T. Mohamed, W. G. Alexander, Z. A. Kellermyer, A. L. Carroll, R. Rossi, I. B. Schlander, G. L. Peabody V, A. M. Guss, A. M. Feist and G. T. Beckham, Evolution and engineering of pathways for aromatic O-demethylation in *Pseudomonas putida* KT2440, *Metab. Eng.*, 2024, **84**, 145–157.

62 J. Zhao, M. Zhu, W. Jin, J. Zhang, G. Fan, Y. Feng, Z. Li, S. Wang, J. S. Lee, G. Luan, Z. Dong and Y. Li, A comprehensive review of unlocking the potential of lignin-derived biomaterials: from lignin structure to biomedical application, *J. Nanobiotechnol.*, 2025, **23**(538)–.

63 Y. Li, Y. Yu, Y. Lou, S. Zeng, Y. Sun, Y. Liu and H. Yu, Hydrogen-Transfer Reductive Catalytic Fractionation of Lignocellulose: High Monomeric Yield with Switchable Selectivity, *Angew. Chem., Int. Ed.*, 2023, **62**, e202307116.

64 W. Jiang, M. A. Wilson and D. P. Weeks, O-demethylations catalyzed by rieske nonheme iron monooxygenases involve the difficult oxidation of a saturated C-H bond, *ACS Chem. Biol.*, 2013, **8**, 1687–1691.

65 E. G. Kovaleva, J. D. Lipscomb, N. Chem and B. Author, Versatility of biological non-heme Fe(II) centers in oxygen activation reactions, *Nat. Chem. Biol.*, 2008, **4**, 186.

66 P. A. Grimsrud, H. Xie, T. J. Griffin and D. A. Bernlohr, Oxidative Stress and Covalent Modification of Protein with Bioactive Aldehydes, *J. Biol. Chem.*, 2008, **283**, 21837.

67 T. Hartmann and S. Leimkühler, The oxygen-tolerant and NAD+-dependent formate dehydrogenase from Rhodobacter capsulatus is able to catalyze the reduction of $CO_2$ to formate, *FEBS J.*, 2013, **280**, 6083–6096.

68 C. E. Foster, T. Krämer, A. F. Wait, A. Parkin, D. P. Jennings, T. Happe, J. E. McGrady and F. A. Armstrong, Inhibition of [FeFe]-hydrogenases by formaldehyde and wider mechanistic implications for biohydrogen activation, *J. Am. Chem. Soc.*, 2012, **134**, 7553–7557.

69 Y. Montet, P. Amara, A. Volbeda, X. Vernede, E. Claude Hatchikian, M. J. Field, M. Frey and J. C. Fontecilla-Camps, Gas access to the active site of Ni-Fe hydrogenases probed by X-ray crystallography and molecular dynamics, *Nat. Struct. Biol.*, 1997, **4**, 523–526.

70 J. Wachtmeister, A. Jakoblinnert, J. Kulig, H. Offermann and D. Rother, Whole-Cell Teabag Catalysis for the Modularisation of Synthetic Enzyme Cascades in Micro-Aqueous Systems, *ChemCatChem*, 2014, **6**, 1051–1058.

71 M. Gaab, S. Bellemin-Laponnaz and L. H. Gade, "Catalysis in a Tea Bag": Synthesis, Catalytic Performance and Recycling of Dendrimer-Immobilised Bis- and Trisoxazoline Copper Catalysts, *Chem. – Eur. J.*, 2009, **15**, 5450–5462.

72 Z. Chen, H. Liu, Q. J. Zong, T. Liang, J. Sun, T. Xu, Z. H. Liu, J. Wu, B. Z. Li and Y. J. Yuan, Engineering Strategies Enabled Protocatechuic Acid Production from Lignin by *Pseudomonas putida* KT2440, *ACS Sustainable Chem. Eng.*, 2024, **12**, 17726–17738.

73 M. E. Runda, H. Miao, N. A. W. de Kok and S. Schmidt, Developing hybrid systems to address oxygen uncoupling in multi-component Rieske oxygenases, *J. Biotechnol.*, 2024, **389**, 22–29.

74 T. Sakai, T. Katsuragi, K. Tonomura, T. Nishiyama and Y. Kawamura, Implantable encapsulated cytosine deaminase having 5-fluorocytosine-deaminating activity, *J. Biotechnol.*, 1985, **2**, 13–21.

75 R. A. Sheldon and S. van Pelt, Enzyme immobilisation in biocatalysis: why, what and how, *Chem. Soc. Rev.*, 2013, **42**, 6223–6235.

76 T. Adachi, T. Miyata, F. Makino, H. Tanaka, K. Namba, K. Kano, K. Sowa, Y. Kitazumi and O. Shirai, Experimental and Theoretical Insights into Bienzymatic Cascade for Mediatorless Bioelectrochemical Ethanol Oxidation with Alcohol and Aldehyde Dehydrogenases, *ACS Catal.*, 2023, **13**(12)), 7955–7965.

Open Access Article. Published on 08 December 2025. Downloaded on 1/7/2026 10:12:59 AM.
This article is licensed under a Creative Commons Attribution 3.0 Unported Licence.

77 P. Tufvesson, J. Lima-Ramos, M. Nordblad and J. M. Woodley, Guidelines and cost analysis for catalyst production in biocatalytic processes, *Org. Process Res. Dev.*, 2011, **15**, 266–274.

78 Y. Wu, C. E. Paul and F. Hollmann, Mirror, mirror on the wall, which is the greenest of them all? A critical comparison of chemo- and biocatalytic oxyfunctionalisation reactions, *Green Carbon*, 2023, **1**, 227–241.

79 R. Li and R. A. Sheldon, The E factor 25 years on: the rise of green chemistry and sustainability, *Green Chem.*, 2017, **19**, 18–43.

80 F. Tieves, F. Tonin, E. Fernández-Fueyo, J. M. Robbins, B. Bommarius, A. S. Bommarius, M. Alcalde and F. Hollmann, Energising the E-factor: The E+-factor, *Tetrahedron*, 2019, **75**, 1311–1314.

81 K. Seelbach and U. Kragl, Nanofiltration membranes for cofactor retention in continuous enzymatic synthesis, *Enzyme Microb. Technol.*, 1997, **20**, 389–392.

82 B. Reus, M. Damian and F. G. Mutti, Advances in cofactor immobilization for enhanced continuous-flow biocatalysis, *J. Flow Chem.*, 2024, **14**, 219–238.

83 A. Kruschitz and B. Nidetzky, Downstream processing technologies in the biocatalytic production of oligosaccharides, *Biotechnol. Adv.*, 2020, **43**, 107568.

84 Y. Li, N. Hu, Z. Xu, Y. Cui, J. Feng, P. Yao, Q. Wu, D. Zhu and Y. Ma, Asymmetric Synthesis of N –Substituted 1,2–Amino Alcohols from Simple Aldehydes and Amines by One–Pot Sequential Enzymatic Hydroxymethylation and Asymmetric Reductive Amination, *Angew. Chem., Int. Ed.*, 2022, **17**, e202116344.

85 S. Güner, V. Wegat, A. Pick and V. Sieber, Design of a synthetic enzyme cascade for the in vitro fixation of a C1 carbon source to a functional C4 sugar, *Green Chem.*, 2021, **23**, 6583–6590.

86 M. Pätzold, S. Siebenhaller, S. Kara, A. Liese, C. Syldatk and D. Holtmann, Deep Eutectic Solvents as Efficient Solvents in Biocatalysis, *Trends Biotechnol.*, 2019, **37**, 943–959.